Evanescent-Wave Fiber-Optic Sensor: On Power Transfer From Core-Cladding Interface to Fiber End-Face

Yasser Chiniforooshan, Jianjun Ma, and Wojtek J. Bock, *Fellow, IEEE*

(Invited Paper)

***Abstract*—In this paper, the enhancement of collection efficiency in fiber-optic evanescent-wave (EW) sensors is studied. Both theory and experimental results are presented. The key is to consider the roughness conditions at the end-face of large-core fibers. The theory is based primarily on ray optics, but for the sake of simplicity and accuracy, wave optics is also considered.**

Fluorescent light is coupled into the core of a partly unclad multimode fiber. Most power is carried to the unclad end-face by tunneling modes. Reflection from this rough end-face, which is modeled as a diffuse source, mixes the initial modes. Bound rays also play an important role, carrying the power to the other end-face. The amount of output power of the bound rays there is calculated. We also study the output power in relation to the surface condition of the far end-face, which may be smooth or rough. The comparison of these cases in terms of output power shows that a rough near end-face enhances the collection of coupled fluorescent light. In contrast, roughening of the far end-face while the near end-face is rough causes a transfer of the initial, mostly tunneling, modes to the radiation modes and decreases the collectable signal.

***Index Terms*—Diffuse source, end-face, evanescent-wave sensors, fiber-optic sensors, fluorescence, ray optics, roughness.**

I. Introduction

FOR a fiber-optic evanescent-wave (EW) sensor, a widely accepted view is that nearly all the power present in the EW arises from the higher-order modes [1], [2]. This explanation would be accurate in small core fibers with few modes excitation. However, in large core fibers, which are been using to improve the fluorescence collection efficiency, with lots of higher order and tunneling modes, the story is different. In this paper, we reveal that this is not a rigorous description of what in fact occurs in propagation of the fluorescence in *large core* fibers, either in ideal or actual one.

Manuscript received July 21, 2011; revised September 12, 2011; accepted September 12, 2011. Date of publication September 22, 2011; date of current version March 21, 2012. This work was supported in part by the Natural Sciences and Engineering Research Council of Canada, in part by the Canada Research Chairs Program, and in part of the Ministère du Développement économique, de l'Innovation et de l'Exportation du Québec, and in part by a NATO Linkage Grant.

The authors are with the Centre de recherche en photonique, Département d'informatique et d'ingénierie, Université du Québec en Outaouais, Gatineau, QC J8X 3X7, Canada (e-mail: chiy03@uqo.ca).

Digital Object Identifier 10.1109/JLT.2011.2168946

In reviewing the literature, we found that few papers have examined the power flow in a simple manner. This is particularly true when several different cladding materials are applied to the fiber core in a cascaded fashion, each of which conditions the power flow. These materials, either polymer or silica, cover most of the fiber length to achieve low attenuation of light transmission over a long distance. There will also be a short air- and/or liquid-clad segment with the latter often representing the liquid sample. A particular difficulty is posed by a sample on the sidewall of the fiber core, since the sample also serves as a specific light source. Light from this source usually radiates isotropically. Its coupling to the core and subsequent detection at the far end (D-end) appears unexplainable in terms of Snell's law and is thus not straightforward from the ray-optics point of view. Explanations of this process often refer to mode theory but tend to be rather complex due to the high density of the modes excited in *large core* fibers. The contribution of this paper lies in its effort to develop a straightforward ray-optics approach to deal with this light coupling problem over the full area from its origin, the source on the surface of the core sidewall, to the remote fiber end-face where the detector or spectrometer is connected.

In particular, both the significant impact of the fiber end-face in the proximal end or S-end—our previously reported discovery [3], [4]—and the effect of the far end on the overall collectable signal level are for the first time simulated theoretically using a light diffuser model. The role of tunneling rays, which are in fact the major contributor to the collectable signal despite being generally ignored in most of the literature, is taken into account as well. We expect this work to provide a more precise and easy-to-follow understanding than has been offered to date of what happens with both ideal and real EW-based fiber-optic sensors.

II. Definitions

A. Classification of the Rays

As a prelude to classification, it is useful to determine the angles θ_z, α and θ_φ which are constants along a particular ray path in the fiber. As illustrated in Fig. 2, θ_z and α refer to the angles of a ray with the z axis and the normal axis, respectively, while α_c is the critical angle and θ_φ is the angle of the projection of a ray on a fiber cross section with azimuth direction. Bound,

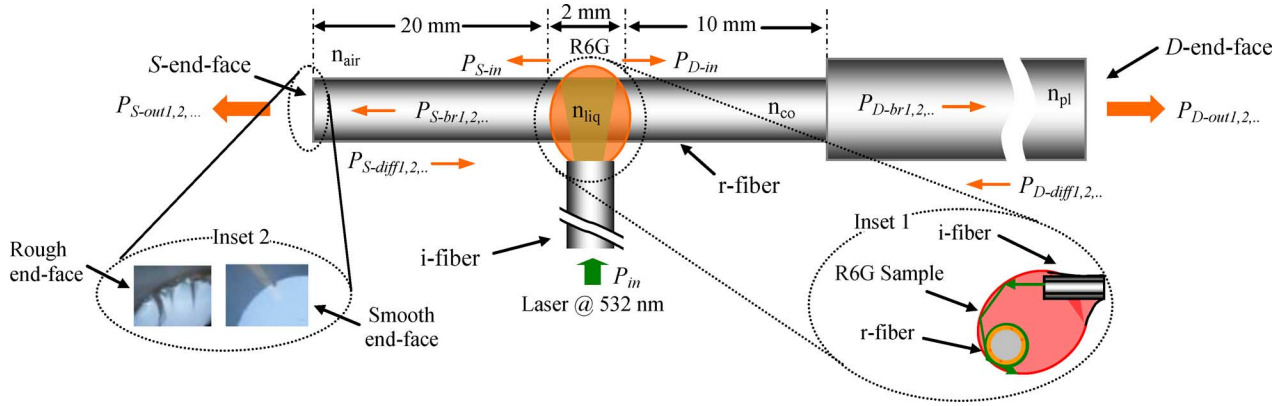

Fig. 1. Powers flow in different segments of a receiving fiber.

refracting and tunneling rays can be specified using these angles, as in the following expressions [5]:

$$\text{Bound rays} : 0 \le \theta_z < \theta_c, \theta_c = \pi/2 - \alpha_c \quad (1)$$

$$\text{Refracting rays} : 0 \le \alpha < \alpha_c \quad (2)$$

$$\text{Tunneling rays} : \theta_c \le \theta_z \le \pi/2 \text{ and } \alpha_c \le \alpha \le \pi/2 \quad (3)$$

B. Experimental setup

As explained in a previous work [6], a different excitation method than the traditional one [7] is used in order to reduce the excitation power background on the detector. Moreover, the fluorescence can be more efficiently collected with this method for two reasons. First, stronger excitation of the fluorophore molecules leads to the release of more fluorescence. Second, in contrast with other methods where a long segment of the fluorescent sample is used, in our method short length of the sample is utilized. In this case, tunneling rays play the main role in the transfer of fluorescence power to the proximal end (S-end). Tunneling rays are a type of skew rays existing because of the curved nature of the fibers. They can contribute significantly to the overall collectable power if the fiber has a large core size.

In our method, the illumination fiber (i-fiber) is perpendicular to and off axis of the receiving fiber (r-fiber). The r-fiber has three segments. The polymer-clad segment is the longest and consists of the fiber with its own regular polymer cladding. The second segment, the area of light coupling into the fiber, is cladded with a liquid. The final segment of the r-fiber is air-clad (Fig. 1).

C. Fluorescence Coupling Mechanism

The polymer cladding of the intended air- and liquid-clad segments is removed using chemical solvent. Fluorophore molecules covering the liquid-clad segment are excited by light entering from the i-fiber and the fluorescence is released isotropically. Then the rays hit the sidewall at an angle within the range of $0 \le \alpha_0 \le \pi/2$, where α_0 is the angle between the outside incident ray and the normal axis as shown in Fig. 2. According to Snell's law, α lies within the range of $0 \le \alpha \le \alpha_{cl}$, where α_{cl} is the critical angle in the liquid-clad segment. Therefore, because of (2), most of the rays penetrating the fiber through the sidewall are refracting rays and only those

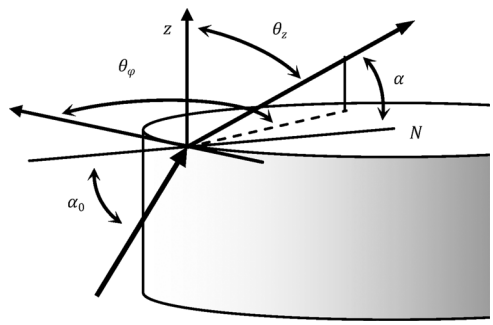

Fig. 2. Ray path invariant angles.

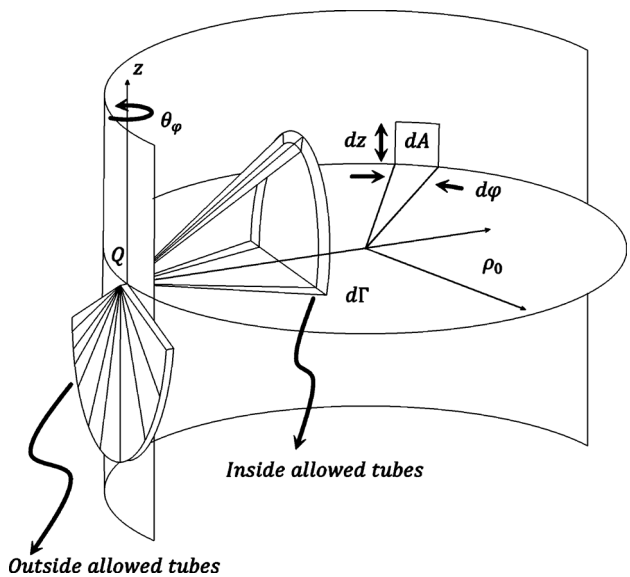

Fig. 3. Fluorescence as a sidewall diffuse source and the tubes which are allowed to penetrate into the fiber from the outside.

that propagate inside the fiber with $\alpha \approx \alpha_{cl}$ can remain as bound or tunneling rays (allowed rays). These inside allowed rays are those outside rays which are tangential to the sidewall of the fiber or have $\alpha_0 = \pi/2$ (Fig. 3).

In the following paragraphs, ray optics is used to describe the power of the light coupled, mixed and propagated inside the fiber.

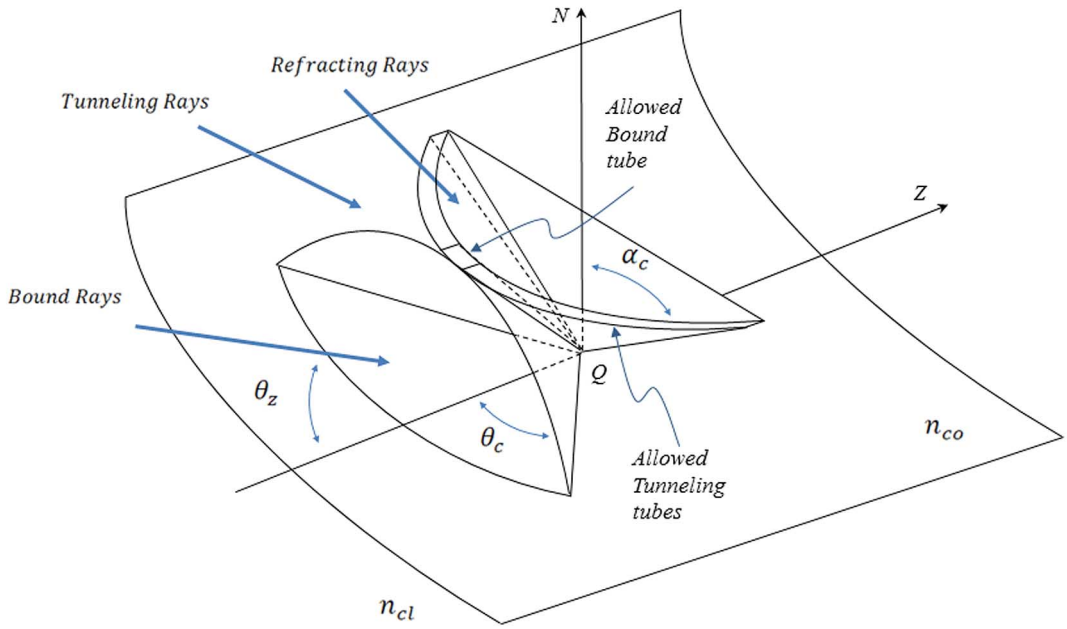

Fig. 4. Tubes which can propagate inside the fiber.

Since the power of an individual ray is undefined, it is useful to introduce the concept of ray tubes. The ray tube is conceived as a tube of rays of infinitesimal cross-section, with each ray propagating in the same direction. Fig. 3 illustrates sample tubes at a point Q on the sidewall that are allowed to penetrate inside the fiber. Fig. 4 shows the point Q in more detail.

In terms of wave optics, it has been shown that those outside waves propagating tangentially to the fiber can couple part of their energy into the fiber via EWs. The thickness of the EW layer is within the range of a hundred nanometers to one wavelength [2]. This means that light can propagate inside the fiber only near its cut-off. These near cut-off modes are tunneling or very-high-order guided modes. In ray optics, these modes are interpreted as rays propagating with an angle $\alpha \approx \alpha_{\rm cl}$ and a thickness δ, which is around one wavelength. Tunneling rays rather than bound rays transfer most of the power along the fiber as shown in Fig. 4.

III. Analysis

Because of the isotropic nature of fluorescence, each differential area of the source emits light in all directions like a diffuse source. But only a small portion of this light can be coupled into the fiber as bound or tunneling rays. The differential power (dP) emitted that is allowed to penetrate into the fiber from a differential area (dA) of the source in a differential solid angle $(d\Gamma)$ in cylindrical coordinates is

$$dP = I_0 d\Gamma dA \tag{4}$$

where I_0 is the intensity of a single ray tube [8]. According to Fig. 3

$$dA = \rho_0 d\varphi dz \tag{5}$$

where ρ_0 is the radius of the fiber core. Focusing on the point Q (Fig. 4), we find that penetrating rays will occupy a differential solid angle

$$d\Gamma = \pi\delta \sin\alpha_{\rm cl} \tag{6}$$

where δ is the thickness of the EW layer.

In a very-large-core fiber, there are thousands of modes which can be excited near the cut-off. As a result, the power in this region seems to be flowing continuously instead of having a discrete modal propagation.

Given that fluorescent light has a totally random direction and because of the symmetry of the structure, we have

$$P_{S-\rm in} = P_{D-\rm in} \tag{7}$$

where $P_{S-\rm in}$ and $P_{D-\rm in}$ represent internal power traveling to the S- and D-ends, respectively. So, the total penetrating power that travels to the S-end is

$$\begin{aligned} P_{S-\rm in} &= \pi\delta \sin\alpha_{\rm cl} \int I_0 \rho_0 d\varphi dz \\ &= \pi I_0 \rho_0 \delta \sin\alpha_{\rm cl} \int_0^{2\pi} d\varphi \int_0^L dz \\ &= 2\pi^2 I_0 \rho_0 L \delta \sin\alpha_{\rm cl} \end{aligned} \tag{8}$$

where L is the length of the liquid-clad segment along the z-axis.

Since the fiber we use is a large-V-number multimode fiber, the critical angle in the polymer-clad segment $(\alpha_{\rm cp})$ is much greater than in the liquid-$(\alpha_{\rm cl})$ or air-clad $(\alpha_{\rm ca})$ segments. So because all allowed rays are near cut-off in the liquid-clad segment or have$\alpha \approx \alpha_{\rm cl}$, the power traveling to the D-end $(P_{D-\rm in})$ is carried by refracting rays in the polymer-clad segment and this power radiates out of the fiber after a while. Then only

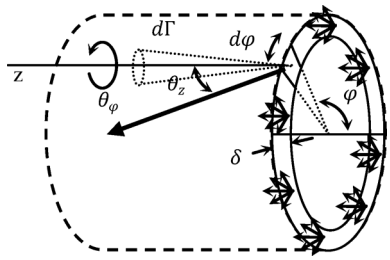

Fig. 5. Random rough surface modeled as a ring-shaped diffuse source near cut-off with a thickness of δ.

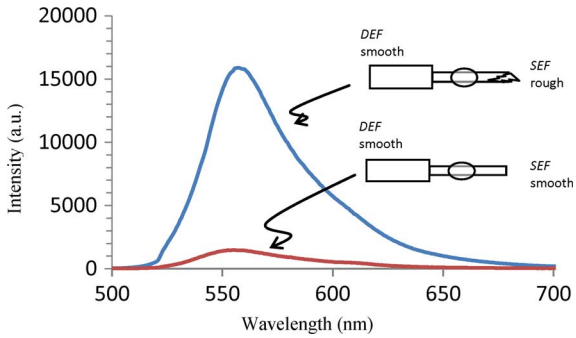

Fig. 6. Output power of fluorescence from D-end-face (DEF) for two fibers. The higher signal is obtained when the S-end-face is rough, while the lower signal is obtained when it is smooth.

$P_{S-\mathrm{in}}$ contributes to the total power collected at the D-end. This portion of the injected power hits the S-end. The roughness of the S-end is important to how the rays reflect back from this end. Accordingly, we now consider two conditions of the S-end-face, rough and smooth.

A. Smooth S-End-Face

The roughness profile of the surface of the smooth S-end-face is less than the light wavelength in size. The rays hitting the S-end-face will exit if $0 \leq \theta_z \leq \alpha_{\mathrm{ca}}$, otherwise they reflect back with the same invariant angles as incident rays and then disappear at the polymer-clad segment for the same reason as $P_{D-\mathrm{in}}$ disappeared. In conclusion, no rays that reach the polymer-clad segment, after reflecting from the *ideal* smooth S-end-face, are allowed to propagate in the polymer-clad part because they are refracting rays in that segment. In this case, no output power exits from the D-end. But in a real case we cannot achieve an *ideally* smooth end-face, and even a small defect can change the output power exiting from the D-end as shown in our experimental results (Fig. 6).

B. Rough S-End-Face

In the case of the rough S-end-face, it is assumed that the roughness is greater than the wavelength. The rays hitting this surface are scattered randomly in almost all directions. This random rough surface can be considered as a diffuse or Lambertian source. Because the light is coupled to the fiber via EW and travels to the S-end just for a few centimeters, the light inside the fiber is assumed to occupy a ring with a radius about equal to the core radius and a thickness equal to that of the EW layer (δ) as illustrated in Fig. 5.

Again referring to Fig. 5, we can calculate the total power of this new source $(P_{S-\mathrm{diff}1,2,\ldots})$ as illustrated in Fig. 1. Generally, parts of the power reflect back and forth inside the fiber for an infinite number of times. The number indexes show those parts in each reflection

$$P_{S-\mathrm{diff}1} = \int_{(\rho_0-\delta)}^{\rho_0} I_1 r dr \int_0^{2\pi} d\varphi \int_0^{\pi/2} \sin\theta_z d\theta_z \int_0^{2\pi} d\theta_\varphi = 2\pi^2 I_1 \left[\rho_0^2 - \rho_0^2(1-\delta/\rho_0)^2\right] = 4\pi^2 I_1 \rho_0 \delta \quad (9)$$

where I_1 is the ray intensity of this source. This total power is related to $P_{S-\mathrm{in}}$ by

$$P_{S-\mathrm{in}} = P_{S-\mathrm{diff}1} + P_{S-\mathrm{out}1} \quad (10)$$

where $P_{S-\mathrm{out}1,2,\ldots}$ are the powers exiting from the S-end. This power is taken to be

$$P_{S-\mathrm{out}1} = \gamma_{S-\mathrm{out}} P_{S-\mathrm{in}}, \quad \gamma_{S-\mathrm{out}} = 1 - \beta_{S-\mathrm{in}} \quad (11)$$

where $\gamma_{S-\mathrm{out}}$ and $\beta_{S-\mathrm{in}}$ are the S-output and -input scattered power coefficients, respectively. Therefore, from (8) to (11)

$$\begin{aligned} P_{S-\mathrm{diff}1} &= (1-\gamma_{S-\mathrm{out}}) P_{S-\mathrm{in}} \\ &= \beta_{S-\mathrm{in}} P_{S-\mathrm{in}} \\ &\Rightarrow 2I_1 = I_0 L \sin\alpha_{\mathrm{cl}} \beta_{S-\mathrm{in}}. \end{aligned} \quad (12)$$

This diffuse source excites all bound, tunneling and refracting rays. The bound rays carry the most of the power over a long distance; however tunneling rays also contribute significantly to the total power in very large core fibers. For simplicity, we focus only on the power carried by the bound rays $(P_{D-\mathrm{br}1,2,\ldots})$ in the polymer-clad segment and traveling from the S-end to the D-end. It can be deduced that every allowed bound ray in the polymer-clad segment is also allowed to propagate in other segments. So according to (1) and (12) we have

$$P_{D-\mathrm{br}1} = \int_{(\rho_0-\delta)}^{\rho_0} I_1 r dr \int_0^{2\pi} d\varphi \int_0^{\theta_{\mathrm{cp}}} \sin\theta_z d\theta_z \int_0^{2\pi} d\theta_\varphi = 4\pi^2 I_0 \rho_0 L \delta \sin\alpha_{\mathrm{cl}} \beta_{S-\mathrm{in}} (1-\cos\theta_{\mathrm{cp}}) \quad (13)$$

where $P_{D-\mathrm{br}1,2,\ldots}$ stand for the power of the bound rays in the polymer-clad segment received from the rough face at the S-end as shown in Fig. 1. Now let us consider the two different types of D-end-face, smooth and rough.

1) Smooth D-End-Face: Due to the fact that the critical angle in the polymer-clad segment is much greater than in the air-clad segment $(\alpha_{\mathrm{cp}} \gg \alpha_{\mathrm{ca}})$ and taking into consideration the bound rays' condition in the polymer-clad segment (1), we can deduce that all power received at the D-end will exit from the fiber, if the D-end-face is *ideally* smooth. So we have

$$P'_{D-\mathrm{out}} = P_{D-\mathrm{br}1} \quad (14)$$

where $P'_{D-\mathrm{out}}$ is the output power from the smooth D-end-face while the S-end-face is rough.

2) Rough D-End-Face: In the case of the rough D-end-face, the rays reaching this end are scattered. A second diffuse source can be assumed at this end-face (D diffuse source) such as the one at the S-end-face (S diffuse source). In contrast with the first

source, this second diffuse source covers the entire area of the D-end-face because this end-face has been totally illuminated by the first diffuse source. The same procedure as for the S diffuse source (12) can be applied to calculate the power of the D diffuse source

$$P_{D-\mathrm{diff1}} = P_{D-\mathrm{br1}}\beta_{D-\mathrm{in}} \tag{15}$$

where $\beta_{D-\mathrm{in}}$ is the D-input scattered power coefficient and $P_{D-\mathrm{diff1,2,...}}$ are the powers of the D diffuse sources in each reflection. It is useful to define the D-output scattered power coefficient $\gamma_{D-\mathrm{out}}$ similar to the one defined for S-end (11). So the first part of the overall output is

$$P_{D-\mathrm{out1}} = P_{D-\mathrm{br1}}\gamma_{D-\mathrm{out}} \tag{16}$$

where $P_{D-\mathrm{out1,2,...}}$ are the output powers from the D-end. We have to remember that the allowed power in the polymer-clad segment is also allowed to propagate in other segments because the critical angle in this segment is much greater than in other segments. Again using the same procedure as was used to calculate $P_{D-\mathrm{br1}}$ (9)–13, we can calculate the power of the bound rays allowed to propagate at the S-end ($P_{S-\mathrm{br1}}$) as

$$P_{S-\mathrm{br1}} = P_{D-\mathrm{diff1}}(1-\cos\theta_{\mathrm{cp}}). \tag{17}$$

This power hits the rough S-end-face and will be scattered again. Thus, we have the second S diffuse source ($P_{S-\mathrm{diff2}}$) which covers the entire area of the S-end. The same procedure as in (15) leads to

$$P_{S-\mathrm{diff2}} = P_{S-\mathrm{br1}}\beta_{S-\mathrm{in}}. \tag{18}$$

Then the allowed part of this power which can reach the D-end is

$$P_{D-\mathrm{br2}} = P_{S-\mathrm{diff2}}(1-\cos\theta_{\mathrm{cp}}). \tag{19}$$

Once this allowed power reaches the D-end, the output part of the power after scattering by the rough D-end-face will be

$$\begin{aligned} P_{D-\mathrm{out2}} &= P_{D-\mathrm{br2}}\gamma_{D-\mathrm{out}} \Rightarrow \\ P_{D-\mathrm{out2}} &= P_{D-\mathrm{br1}}\beta_{D-\mathrm{in}}(1-\cos\theta_{\mathrm{cp}})\beta_{S-\mathrm{in}} \\ &\quad \times (1-\cos\theta_{\mathrm{cp}})\gamma_{D-\mathrm{out}}. \end{aligned} \tag{20}$$

This back and forth reflection and scattering from the S- and D-end-faces continues for an infinite number of times. Each time, some portion of the power exits from the S- and D-end-faces. Following the same procedure, the total output power from the D-end-face is calculated as

$$\begin{aligned} P_{D-\mathrm{out}} &= P_{D-\mathrm{br1}}\gamma_{D-\mathrm{out}} \\ &\quad \times \sum_{i=0}^{\infty}\{\beta_{D-\mathrm{in}}\beta_{S-\mathrm{in}}(1-\cos\theta_{\mathrm{cp}})^2\}^i. \end{aligned} \tag{21}$$

This is a well known geometric series. Since the argument of the sigma is less than one, $\beta_{D-\mathrm{in}}\beta_{S-\mathrm{in}}(1-\cos\theta_{\mathrm{cp}})^2 < 1$, then the summation has a finite answer which is

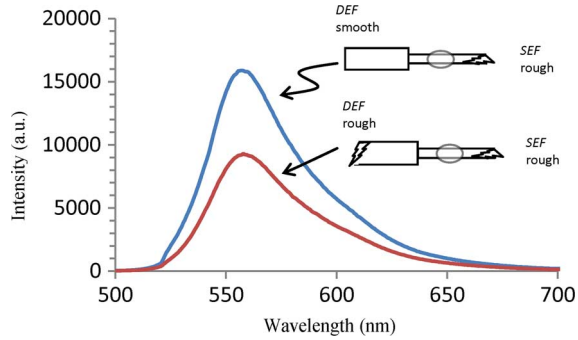

Fig. 7. Output power of fluorescence from the D-end-face (DEF) for two fibers. In the case of the higher signal, the D-end-face is smooth while for the lower signal, the D-end-face is rough. The S-end-face (SEF) is rough in both cases.

$$\begin{aligned} P_{D-\mathrm{out}} &= P_{D-\mathrm{br1}}\gamma_{D-\mathrm{out}} \\ &\quad \times \frac{1}{1-\beta_{D-\mathrm{in}}\beta_{S-\mathrm{in}}(1-\cos\theta_{\mathrm{cp}})^2}. \end{aligned} \tag{22}$$

The output power of this fiber (both S- and D-end-faces are rough) can be compared with the output power from the fiber with a rough S-end-face and a smooth D-end-face. From (14) and (22) we have

$$\begin{aligned} \frac{P'_{D-\mathrm{out}} - P_{D-\mathrm{out}}}{P'_{D-\mathrm{out}}} \\ = \frac{1-\gamma_{D-\mathrm{out}}}{1-\beta_{D-\mathrm{in}}\beta_{S-\mathrm{in}}(1-\cos\theta_{\mathrm{cp}})^2}. \end{aligned} \tag{23}$$

In the most general and simple case, one can assume that each point of the diffuse source acts as a point-light-source which radiates its intensity equally in all directions. In this case all β and γ are equal to $1/2$. By assuming the fiber is a step-index multimode fiber with a core/cladding size of 400/430 μm and an NA of 0.37, we can calculate this ratio (23) as $P'_{D-\mathrm{out}} - P_{D-\mathrm{out}}/P'_{D-\mathrm{out}} = 0.5$, which means that roughening the D-end-face on a sensor with an already roughened S-end-face decreases the signal collectability to 50%. This is the so-called over-mixing effect at the D-end-face. This finding will be proven by our experimental data discussed in the next section and shown in Fig. 7.

IV. Experimental Results

A Rhodamine 6G (R6G) sample droplet described in [6] is dispensed on the unclad sidewall of the fiber to form the liquid-clad segment. Fluorescence, centered around 555 nm, is coupled into the fiber using our EW fiber-optic fluorometer platform as shown in Fig. 1. Experimental data was obtained for two different S- and D-end-faces, smooth and rough. We prepared these end-faces by polishing them with the standard Buehler® Fibermet® discs. To achieve the smooth end-face we used a 0.3 μm disc, close to half the wavelength in size, while for the rough end-face we used a 12 μm disc, more than twenty times larger than the wavelength.

Fig. 6 shows the output powers from the D-end for smooth and rough S-end-faces while the other end of both fibers is smooth.

As we explained theoretically in the previous section, the roughened S-end-face contributes to the collection of fluorescence to a much greater extent than the smooth S-end-face. However, as expected, there is some light even in the case of the smooth S-end-face due to its non-ideally polished condition. So in real, the fluorescence collectability in this case increases by 91% if the S-end-face is rough.

Fig. 7 shows the effect of the D-end-face condition on collectable fluorescence power.

The lower power is collected from the fiber with two rough ends while the higher power is collected from the fiber with a rough S- end-face and a smooth D-end-face. This experimental result shows that the collectability of the sensor decreases to 42% by roughening the D-end-face on a sensor with an already roughened S-end-face. This amount was calculated using simplification in Section III.B.2 by 50%.

V. Conclusion

In this article, we first showed theoretically the effect of S- and D-end-face roughness on the efficiency of a fiber-optic EW sensor in collecting EW fluorescent light and then confirmed the effect experimentally. This study shows that scattering from a rough S-end-face enhances the EW collection in the opposite end of the sensor by mixing the initial modes, which are mostly tunneling, into a combination of tunneling and bound modes.

People traditionally focus on the sensing end-face to enhance fluorescence collection. In contrast, we have shown theoretically that the D-end-face condition is involved in measurable fluorescent power. The evidence of our experimental results presented in Fig. 7 supports this finding. The signal achieved by the fiber with the rough D-end-face is lower than the signal received from the fiber with the smooth D-end-face when the S-end-face is rough in both cases. The brief explanation of this phenomenon is that the rough D-end-face causes over-mixing of the modes already mixed by the rough S-end-face.

References

[1] B. D. MacCraith, "Enhanced evanescent wave sensor based on sol-gel-derived porous glass coatings," *Sens. Actuators B*, vol. 11, pp. 29–34, 1993.

[2] C. R. Taitt, G. P. Anderson, and F. S. Ligler, "Evanescent-wave fluorescence biosensors," *Biosens. Bioelectron.*, vol. 20, pp. 2470–2487, 2005.

[3] J. Ma, Y. Chiniforooshan, and W. J. Bock, "Rerouting end-face-TIR capable rays to significantly increase evanescent wave signal power," *Chin. Opt. Lett.*, vol. 9, no. 4, p. 040603, 2011.

[4] J. Ma, W. J. Bock, and A. Cusano, "Insights into tunnelling rays: Outperforming guided rays in fiber-optic sensing device," *Opt. Exp.* vol. 17, pp. 7630–7639, 2009 [Online]. Available: http://www.opticsinfobase.org/oe/abstract.cfm?URI=oe-17-9-7630

[5] A. W. Snyder and J. D. Love, *Optical Waveguide Theory*. London, U.K.: Chapman and Hull Ltd., 1983, ch. 2, pp. 29–31.

[6] J. Ma and W. J. Bock, "Reshaping sample fluid droplet: Towards combined performance enhancement of evanescent-wave fiber-optic fluorometer," *Opt. Lett.*, vol. 32, pp. 8–10, 2007.

[7] A. Leung, P. M. Shankar, and R. Mutharasan, "A review of fiber-optic biosensors," *Sens. Actuators B*, vol. 125, pp. 688–703, 2007.

[8] A. W. Snyder and J. D. Love, *Optical Waveguide Theory*. London, U.K.: Chapman and Hull Ltd., 1983, ch. 4.

Yasser Chiniforooshan received the B.S. degree in physics from Shiraz University, Shiraz, Iran, in 1998 and the M.S. degree of photonics from laser research institute of Shahid Beheshti University Tehran, Iran, in 2001. Currently, he is working towards the Ph.D. degree in electrical engineering at the photonic Research Center (PRC), Department of information and engineering, Université du Québec en Outaouais (UQO), Gatineau, QC, Canada.

His research interest is optical fiber evanescent-wave sensors, surface plasmon fiber sensors, fiber grating sensors and their applications in bio/environmental hazard detection.

Wojtek J. Bock (M'85–SM'90–F'03) received the M.Sc. degree in electrical engineering and the Ph.D. in solid state physics from the Warsaw University of Technology, Poland, in 1971 and 1980, respectively.

Since 1989 he has been a full Professor of Electrical Engineering at the Université du Québec en Outaouais (UQO), Canada. Since 2003, he has been a Canada Research Chair Tier-I in Photonics and the Director of the Photonics Research Center at UQO. His research interests include fiber-optic sensors and devices, multisensor systems, and systems for precise measurement of non-electric quantities. He has authored and co-authored more than 270 scientific papers, patents and conference papers in the fields of fiber optics and metrology which have been cited about 350 times.

Prof. Bock is an Associate Editor of the IEEE/OSA Journal of Lightwave Technology and the International Journal of Optics.